Mon. Not. R. Astron. Soc. **000**, 000–000 (0000) Printed 5 February 2008 (MN LATEX style file v2.2)

R modes of slowly pulsating B stars

Umin Lee[1] ⋆
[1] *Astronomical Institute, Tohoku University, Sendai, Miyagi 980-8578, Japan*

Typeset 5 February 2008; Received / Accepted

ABSTRACT

Slowly pulsating B (SPB) stars are g mode pulsators in main-sequence stages with mass ranging from $M \sim 3M_\odot$ to $\sim 8M_\odot$. In this paper, we examine pulsational stability of low m r modes in SPB stars by calculating fully nonadiabatic oscillations of uniformly rotating stars, where m is an integer representing the azimuthal wave number around the rotation axis. R modes are rotationally induced, non-axisymmetric, oscillation modes, whose oscillation frequency strongly depends on the rotation frequency Ω of the star. They are conveniently classified by using two integer indices m and $l' \geq |m|$ that define the asymptotic oscillation frequency $2m\Omega/[l'(l'+1)]$ in the limit of $\Omega \to 0$. We find low m, high radial order, odd r modes with $l' = m$ in SPB stars are excited by the same iron opacity bump mechanism that excites low frequency g modes of the variables, when the rotation frequency Ω is sufficiently high. No even r modes with low m are found to be pulsationally unstable. Since the surface pattern of the temperature perturbation of odd modes is antisymmetric about the equator of the star, observed photometric amplitudes caused by the unstable odd r modes with $l' = m$ are strongly dependent on the inclination angle between the axis of rotation and the line of sight. Applying the wave-meanflow interaction formalism to nonadiabatic r modes in rapidly rotating SPB models, we find that because of the $r\phi$ component of the Reynolds stress and the radial transport of the eddy fluctuation of density in the rotating star, the surface rotation is accelerated by the forcing due to the low $l' = m$ unstable r modes. We suggest that the amount of angular momentum redistribution in the surface region of the stars can be comparable to that needed to sustain decretion discs found in Be systems.

We make a brief comparison between nonadiabatic r mode calculations done with and without the traditional approximation. In the traditional approximation, the local horizontal component of the rotation vector $\mathbf{\Omega}$ is ignored in the momentum conservation equation, which makes it possible to represent the angular dependence of an oscillation mode using a single Hough function. We find that the oscillation frequencies of low m r modes computed with and without the traditional approximation are qualitatively in good agreement. We also find that the pulsational instability of r modes in the traditional approximation appears weaker than that without the approximation.

Key words: stars: oscillations – stars : rotation

1 INTRODUCTION

Slowly pulsating B stars (hereafter SPB stars) are g mode pulsators (e.g., Waelkens 1991, Waelkens et al 1998). Low frequency g mode oscillations in SPB stars are excited by the iron opacity bump mechanism, which also excites high frequency p modes in β Cephei stars (Dziembowski & Pamyatnykh 1993; Dziembowski, Moskalik, & Pamyatnykh 1993; Gautschy & Saio 1993, see also Kiriakidis, ElEid, & Glatzel 1992). Savonije (2005) and Townsend (2005b) have recently shown that low m r modes in SPB stars are also excited by the same opacity bump mechanism that excites g modes, if rapid rotation is assumed. Although SPB stars are not necessarily rapid rotators, a fraction of SPB stars are rapidly rotating (e.g., Aerts et al 1999). Rapidly

⋆ E-mail: lee@astr.tohoku.ac.jp

rotating SPB stars will be good observational targets for both g mode and r mode oscillations, which can be used as a probe to investigate the interior structure of the variables.

R modes are rotationally induced, non-axisymmetric, low frequency oscillation modes whose toroidal component of the displacement vector is dominant over the horizontal and the radial components, and whose oscillation frequency is proportional to the rotation frequency Ω (e.g., Papaloizou & Pringle 1978; Provost, Berthomieu, & Rocca 1981; Saio 1982; Berthomieu & Provost 1983). R modes are retrograde modes in the corotating frame of the star, but are prograde when seen in an inertial frame. In the limit of $\Omega \to 0$, the displacement vector is well represented by a single spherical harmonic function $Y_{l'}^m$ and the oscillation frequency ω observed in the corotating frame of the star tends to the asymptotic frequency given by $\omega_c(m, l') \equiv 2m\Omega/[l'(l'+1)]$ with $l' \geq |m|$. R modes are therefore conveniently classified by using the two integer indices m and $l'(\geq |m|)$ that define the asymptotic freqyency $\omega_c(m, l')$. For a neutrally-stratified (isentropic) star, in which the Brunt-Väisälä frequency N vanishes identically in the interior, the odd r mode with $l' = m$ that has no radial nodes of the eigenfunction is the only r mode we can find for given m and Ω (see, e.g, Saio 1982, Lockitch & Friedman 1999, Yoshida & Lee 2000a). The restoring force for the r mode is exclusively attributable to the Coriolis force. For a stably-stratified star, however, buoyant force comes into play as an additional restoring force for the low frequency oscillations. For any combination of m, $l'(\geq |m|)$, and Ω, there exist an infinite sequence of r modes that differ in the number of radial nodes of the eigenfunction (e.g., Yoshida & Lee 2000b). In this paper, we shall call r modes in stably-stratified stars buoyant r modes.

For r modes to be pulsationally excited in SPB stars, rapid rotation of the star is required (Savonije 2005, Townsend 2005b). Expecting a fraction of SPB stars are rapidly rotating, and noting that some Be stars are found in the SPB domain in the HR diagram, it may be reasonable to expect that there exists a link between a class of Be stars and rapidly rotating SPB stars. Be stars are characterized by emission lines, which are thought to have their origin in the gaseous discs surrouonding the central B stars. Time variability of the emission lines in strength and shape as well as their appearance and dissapearance are believed to be closely related to the dynamical status of the gaseous discs aurrounding the stars (see a recent review by Porter & Rivinius 2003). Although discs around Be stars are indispensable for observed Be phenomena, no definite physical mechanisms responsible for disc formation have not so far been indentified. Considering that both g modes and r modes become pulsationally unstable in rapidly rotating SPB stars, it is tempting to speculate these low frequency oscillation modes play a role in angular momentum transfer in the interior that leads to disc formation around the stars. To investigate angular momentum redistribution in rotating stars, in a series of papers Ando (1981, 1982, 1983, 1986) has applied to stellar pulsations the wave-meanflow intercation formalism, which has been extensively used in geophysics and fluid mechanics (e.g., Lighthill 1978; Craik 1985; Pedlosky 1987; Andrews, Holton, & Leovy 1987). Carring out a numerical simulation, Ando (1986) has argued that quasi-periodic vacillation phenomena in Be stars occur as a result of the interaction between the rotation and two prograde and retrograde global oscillation modes. Quite similar calculation has also been done to simulate the quasi-biennial oscillation in the earth's atmosphere (Plumb 1977; see also Lindzen & Holton 1968). We think it worthwhile to apply the wave-meanflow interaction formalism to pulsationally unstable low frequency modes in rapidly rotating SPB stars, speculating that unstable prograde and retrograde g modes are responsible for quasi-periodioc vacillations, and unstable r modes are working as a stable angular momentum supplier to the surrounding discs.

In the analyses of nonadiabatic oscillations of SPB stars, Savonije (2005) and Townsend (2005a,b) exclusively used the traditional approximation, neglecting the local horizontal component of the rotation vector $\mathbf{\Omega}$ in the momentum conservation equation (e.g., Eckart 1960). In the traditional approximation, separation of variables between spherical polar coordinates (r, θ, ϕ) becomes possible and the governing equations for oscillations in rotating stars are largely simplified (e.g., Lee & Saio 1987a). The traditional approximation has been extensively employed in geophysics to study waves propagating in an atmospheric or ocean fluid layer that is very thin campared to the radius of the earth. The approximation is thought to be valid for low frequency oscillations with $\omega << N$ so that the horizontal component of the fluid velocity is much larger than the radial component (e.g., Eckart 1960). When we apply the traditional approximation to global oscillations of rotating stars, however, validity of the approximation is not very clear, since the condition $\omega << N$ may not always be satisfied in the entire interior, for example. In this paper, we calculate nonadiabatic low m buoyant r modes of SPB stars without applying the traditional approximation, in order to examine their pulsational stability. We also apply the wave-meanflow interaction formalism to nonadiabatic r modes to see if acceleration of the surface rotation is possible as a result of the forcing. The result of the stability analysis is given in §3 and the wave-meanflow interaction for the r modes is discussed in §4. A brief comparison between nonadiabatic r mode calculations with and without the traditional approximtion is given in §5. We briefly describe our numerical method in §2, and conclusions are summarized in §6.

2 NUMERICAL METHOD

The numerical method of calculating nonadiabatic oscillations of uniformly rotating stars is the same as that given in Lee & Saio (1987b, 1993). We employ a linear theory of oscillations to describe small amplitude pulsations of rotating stars. We assume that the background state of rotating stars is axisymmetric about the rotation axis, and that the time t and

azimuthal angle ϕ dependence of perturbations to the background state is given by $\exp[i(\sigma t + m\phi)]$, where σ is the oscillation frequency in an inertial frame, and m is an integer representing the azimuthal wavenumber around the rotation axis. Under these assumptions, linearized hydrodynamic equations are given by

$$-\omega^2\rho\boldsymbol{\xi} + 2\mathrm{i}\omega\rho\boldsymbol{\Omega}\times\boldsymbol{\xi} = -\nabla p' - \rho'\nabla\Phi - \rho\nabla\Phi', \tag{1}$$

$$\rho' + \nabla\cdot(\rho\boldsymbol{\xi}) = 0, \tag{2}$$

$$\nabla^2\Phi' = 4\pi G\rho', \tag{3}$$

$$\mathrm{i}\omega\rho T\delta s = (\rho\epsilon - \nabla\cdot\boldsymbol{F})', \tag{4}$$

and

$$\frac{\delta p}{p} = \Gamma_1\frac{\delta\rho}{\rho} + \alpha_T\Gamma_1\frac{\delta s}{c_p}, \tag{5}$$

where ρ is the mass density, p is the pressure, T is the temperature, s is the specific entropy, c_p is the specific heat at constant pressure, Φ is the gravitational potential, $\boldsymbol{F}$ is the energy flux vector, ϵ is the nuclear energy generation rate per unit mass, $\boldsymbol{\Omega}$ is the vector of angular velocity of rotation,

$$\omega \equiv \sigma + m\Omega \tag{6}$$

is the oscillation frequency observed in the corotating frame of the star, and

$$\Gamma_1 = \left(\frac{\partial\ln p}{\partial\ln\rho}\right)_s, \quad \alpha_T = -\left(\frac{\partial\ln\rho}{\partial\ln T}\right)_p. \tag{7}$$

Here, $\boldsymbol{\xi}$ is the displacement vector, and the quantities attached by a prime ($'$) and δ represents their Eulerian and Lagrangian perturbations, respectively. The total energy flux is given as $\boldsymbol{F} = \boldsymbol{F}_{\rm conv} + \boldsymbol{F}_{\rm rad}$, where $\boldsymbol{F}_{\rm conv}$ is the convective energy flux, which is calculated using a mixing length theory of turbulent convection, and $\boldsymbol{F}_{\rm rad}$ denotes the radiative energy flux given by

$$\boldsymbol{F}_{\rm rad} = -\frac{ac}{3\kappa\rho}\nabla T^4, \tag{8}$$

where κ is the opacity, and a and c denote the radiative constant and the velocity of light, respectively. For the pertubation of the convective flux, we assume $\delta(\nabla\cdot\boldsymbol{F}_{\rm conv}) = 0$ for simplicity.

We apply boundary conditions both at the surface and at the center of the star. The surface boundary conditions we use at $r = R$ are $\delta p = 0$, $\delta(L_r - 4\pi r^2\sigma_{\rm SB}T^4) = 0$, and the condition that Φ' is continuous at the stellar surface, where $L_r = 4\pi r^2 F_r$ is the luminosity at r, and $\sigma_{\rm SB}$ is the Stefan-Boltzmann constant. The inner boundary conditions at $r = 0$, on the other hand, come from the regularity condition of the mechanical variables at the center and from the condition that oscillations are nearly adiabatic, $\delta s/c_p \sim 0$, in the deep interior.

In this paper, we employ a spherical polar coordinate system (r,θ,ϕ) whose origin is at the center of the star and the axis of $\theta = 0$ is along the rotation axis. For a given m, the displacement vector $\boldsymbol{\xi}(r,\theta,\phi,t)$ is given by a truncated series expansion in terms of spherical harmonic functions $Y_l^m(\theta,\phi)$ with different l's as

$$\frac{\xi_r}{r} = \sum_{j=1}^{j_{\rm max}} S_{l_j}(r)Y_{l_j}^m(\theta,\phi)e^{i\sigma t}, \tag{9}$$

$$\frac{\xi_\theta}{r} = \sum_{j=1}^{j_{\rm max}}\left[H_{l_j}(r)\frac{\partial}{\partial\theta}Y_{l_j}^m(\theta,\phi) + \frac{T_{l'_j}(r)}{\sin\theta}\frac{\partial}{\partial\phi}Y_{l'_j}^m(\theta,\phi)\right]e^{i\sigma t}, \tag{10}$$

$$\frac{\xi_\phi}{r} = \sum_{j=1}^{j_{\rm max}}\left[\frac{H_{l_j}(r)}{\sin\theta}\frac{\partial}{\partial\phi}Y_{l_j}^m(\theta,\phi) - T_{l'_j}(r)\frac{\partial}{\partial\theta}Y_{l'_j}^m(\theta,\phi)\right]e^{i\sigma t}, \tag{11}$$

and the pressure perturbation, $p'(r,\theta,\phi,t)$, for example, is given as

$$p' = \sum_{j=1}^{j_{\rm max}} p'_{l_j}(r)Y_{l_j}^m(\theta,\phi)e^{i\sigma t} \tag{12}$$

where $l_j = |m| + 2(j-1)$ and $l'_j = l_j + 1$ for even modes and $l_j = |m| + 2j - 1$ and $l'_j = l_j - 1$ for odd modes where $j = 1,\ 2,\ \cdots,\ j_{\rm max}$. Note that the function p' is symmetric (antisymmetric) for even (odd) modes about the equator of the star. Substituting the expansions (9) to (12) into linearized hydrodynamic equations (1) to (5), we obtain a set of coupled linear ordinary differential equations of a finite dimension $j_{\rm max}$ for the radial expansion functions. With the boundary conditions at the center and at the surface of the star, we solve the set of linear differential equations of a finite dimension as an eigenvalue

problem for the oscillation frequency ω (Lee & Saio 1987b, 1993). Oscillation modes with $\omega_{\rm I} = {\rm Im}(\omega) < 0$ are pulsationally unstable while those with $\omega_{\rm I} > 0$ stable. Note that we do not include terms associated with the centrifugal force, that is, setting $f = 0$ in the oscillation equations given in Lee & Saio (1987b, 1993).

If ω and $\boldsymbol{\xi}$ are respectively the eigenfrequency and the eigenfunction of a mode governed by the oscillation equations (1) to (5), multiplying equation (1) by $\boldsymbol{\xi}^*$, which is the complex conjugate of the displacement vector $\boldsymbol{\xi}$, and integrating over the whole volume of the star, we obtain

$$\omega^2 E + 2\omega F - G = 0, \tag{13}$$

where

$$E = \int \rho \boldsymbol{\xi}^* \cdot \boldsymbol{\xi} dV, \tag{14}$$

$$F = -{\rm i} \int \rho \boldsymbol{\xi}^* \cdot (\boldsymbol{\Omega} \times \boldsymbol{\xi})\, dV, \tag{15}$$

$$G = \int \boldsymbol{\xi}^* \cdot \left(\nabla p' + \rho' \nabla \Phi + \rho \nabla \Phi' \right) dV. \tag{16}$$

Note that E and F are real quantities, because $(\boldsymbol{\xi}^* \cdot \boldsymbol{\xi})^* = \boldsymbol{\xi}^* \cdot \boldsymbol{\xi}$ and $[{\rm i}\boldsymbol{\xi}^* \cdot (\boldsymbol{\Omega} \times \boldsymbol{\xi})]^* = {\rm i}\boldsymbol{\xi}^* \cdot (\boldsymbol{\Omega} \times \boldsymbol{\xi})$. Since the term G can be rewritten as

$$G = \int dV \left[\frac{1}{\Gamma_1} \frac{\delta p^*}{p} \delta p - \left(\frac{\delta \rho^*}{\rho} \boldsymbol{\xi} \cdot \nabla p + \frac{\delta \rho}{\rho} \boldsymbol{\xi}^* \cdot \nabla p \right) + \frac{(\boldsymbol{\xi} \cdot \nabla \rho)(\boldsymbol{\xi}^* \cdot \nabla p)}{\rho} - \frac{\nabla \Phi' \cdot \nabla \Phi'^*}{4\pi G} - \alpha_T \delta p \frac{\delta s^*}{c_p} \right]$$
$$+ \int d\boldsymbol{S} \cdot \left(\boldsymbol{\xi}^* p' + \rho \boldsymbol{\xi}^* \Phi' + \Phi' \frac{\nabla \Phi'^*}{4\pi G} \right), \tag{17}$$

substituting $\omega = \omega_{\rm R} + {\rm i}\omega_{\rm I}$ into equation (13), we obtain

$$\omega_{\rm I} = \frac{1}{2(\omega_{\rm R} E + F)} \int {\rm Im} \left(-\alpha_T \delta p \frac{\delta s^*}{c_p} \right) dV, \tag{18}$$

where we have assumed that ∇p is parallel to $\nabla \rho$ and that the surface terms can be ignored because of the outer boundary conditions employed in this paper. For oscillations of rotating stars, we may define a work integral as

$$w(r) = -\frac{1}{2(\omega_{\rm R} E + F)} \int_0^r {\rm Im} \left(-\alpha_T \delta p \frac{\delta s^*}{c_p} \right) 4\pi r^2 dr, \tag{19}$$

so that we have $w(R) > 0$ for unstable modes having $\omega_{\rm I} < 0$. We can use $w(R)$ as a check on numerical consistency in nonadiabatidc calculations. As $\Omega \to 0$, $F \to 0$, and the work integral (19) reduces to that for non-rotating stars. We note that the region in which $dw(r)/dr > 0$ is a driving region for the oscillation while the region of $dw(r)/dr < 0$ a damping region.

3 MODAL PROPERTY OF R MODES IN SPB STARS

Main sequence models used for pulsation calculation are computed with a standard stellar evolution code, into which we incorporate the opacity tables computed by Iglesias, Rogers, & Wilson (1992), and Iglesias and Rogers (1996). Figure 1 shows evolutionary tracks, from the ZAMS to early hydrogen shell burning stages, of stars having $M = 3M_\odot$ to $M = 8M_\odot$ for $X = 0.7$ and $Z = 0.02$, where the circles are SPB stars tabulated in Waelkens et al (1998) and the filled circles indicate rapidly rotating SPB stars given in Aerts et al (1999).

We classify buoyant r modes using two integer indices m and $l' (\geq |m|)$ that define the asymptotic frequency $\omega_c(m, l') \equiv 2m\Omega/[l'(l'+1)]$ for a given Ω. Note that the mixed modes discussed by Townsend (2005b) correspond to the odd r modes with $l' = m$ in our classification. For given (m, l'), we introduce an integer index n to indicate the radial order of the mode, and we write r_n and/or ω_n to denote the n th radial order r mode. The integer n usually corresponds to the number of radial nodes of the eigenfunction. In this paper we exclusively assume $m > 0$. Then in our convention, the r mode frequency ω observed in the corotating frame is positive, and the frequency σ in an inertial frame is negative. For given (m, l') and Ω, the asymptotic frequency ω_c also sets the upper limit to the r mode frequencies in the sense that $\omega_c(m, l') > \omega_0 > \omega_1 > \omega_2 > \cdots$ (but see also Yoshida & Lee 2000a). We may call r_0 with ω_0 the fundamental r mode. R modes with $\omega_n \cong \omega_c$ have almost solenoidal displacement vector, so that $\nabla \cdot \boldsymbol{\xi} = -\delta\rho/\rho \sim 0$ and hence $\delta p/p \sim 0$ in the interior.

3.1 Pulsational stability of buoyant r modes

We calculate nonadiabatic low m r modes of uniformly rotating stars in main-sequence stages for $M = 3M_\odot$ to $8M_\odot$ for $X = 0.7$ and $Z = 0.02$. As a typical example of SPB stars, we mainly discuss the case for the $5M_\odot$ main-sequence models.

The results for *odd* r modes with $l' = m = 1$ and 2 for $\bar{\Omega} = \Omega/\sqrt{GM/R^3} = 0.4$ are given in Figures 2 and 3, respectively, where the dimensionless oscillation frequency $\bar{\omega}_{\rm R} \equiv \omega_{\rm R}/\sqrt{GM/R^3}$ is plotted as a function of $\mathrm{Log}T_{\rm eff}$ with $T_{\rm eff}$ being the effective temperature from the ZAMS to the TAMS. Here, the small thin and large thick circles indicate pulsationally stable and unstable modes, respectively. Note that the dimensionless limiting frequencies $\bar{\omega}_c(m, l')$ for the r modes with $l' = m = 1$ and 2 are respectively $\bar{\omega}_c = 0.4$ and 0.2666 for $\bar{\Omega} = 0.4$. Figure 4 is the same as Figure 2 but for $\bar{\Omega} = 0.2$, for which $\bar{\omega}_c = 0.2$. Since the oscillation frequency ω of r modes is essentially proportional to Ω, the angular rotation frequency as large as $\bar{\Omega} \gtrsim 0.1$ is necessary for the r modes to be effectively excited by the opacity bump mechanism. As shown by these figures, only high radial order r_n modes having $n >> 1$ become pulsationally unstable. As the star evolves from the ZAMS to the TAMS, the frequency range and the number of unstable r modes of the $5M_\odot$ star gradually increases and the frequency spectrum becomes denser, reflecting the developement of the μ (mean-molecular-weight) gradient zone just outside the convective core. Note that all the r modes are stabilized before the star goes into shell hydrogen burning stages. Compared with the case of $\bar{\Omega} = 0.2$, the width of $T_{\rm eff}$ for unstable r modes is wider for $\bar{\Omega} = 0.4$ in the HR diagram, suggesting that rapid rotation favors the excitation of r modes.

As found from Figures 2 to 4, in the course of evolution from ZAMS, the fundamental r_0 modes with $l' = m$, which behave like an interface mode having the maximum amplitude at the interface between the convective core and the radiative envelope, become unstable because of the ϵ mechanism (see also Townsend 2005b). The growth rates $\eta \equiv -\omega_{\rm I}/\omega_{\rm R}$ of the modes, however, are of order of 10^{-12} to 10^{-11}, and the unstable fundamental r_0 modes may not have important observational consequences.

In Figure 5, we plot, as an example, the work integral $w(r)$ for a unstable odd r_{20} mode with $l' = m = 1$ of a $5M_\odot$ model with $\mathrm{Log}T_{\rm eff} = 4.188$ for $\bar{\Omega} = 0.4$. In this figure, we also plot $\kappa_{\rm ad} = (\partial \ln \kappa/\partial \ln p)_{\rm ad}$ versus r/R for the model. Strong excitation for the r_{20} mode occurs in an outer envelope region where $d\kappa/dr$ is positive, and overcomes damping effects in the deep interior. In Figure 6, the growth rate η of unstable r modes with $l' = m = 1$, 2, and 3 of the $5M_\odot$ model with $\mathrm{Log}T_{\rm eff} = 4.188$ is plotted versus the inertial frame oscillation frequency $|\sigma|$ for $\bar{\Omega} = 0.4$ (0.0118mHz), where the two filled wedges on the horizontal axis indicates the rotation frequencies Ω and 2Ω. The r modes with $l' = m = 1$ have on average larger growth rates, compared to those of the r modes with $l' = m = 2$ and 3.

In Figure 7, we plot $\bar{\omega}_{\rm R}$ of *even* r modes with $l' = m + 1 = 2$ versus $\mathrm{Log}T_{\rm eff}$ for $\bar{\Omega} = 0.4$. No pulsationally unstable r modes with even parity are found. This may be attributable to the fact that the even r modes with $l' = m+1 = 2$ for a given Ω have frequencies by about a factor of 3 smaller than those of the odd r modes with $l' = m = 1$. In fact, we have tried to find unstable even r modes assuming $\bar{\Omega} = 0.8$, but failed. Figure 8 depicts the work integral $w(r)$ of an even r_{20} mode with $l' = m + 1 = 2$ of the $5M_\odot$ model with $\mathrm{Log}T_{\rm eff} = 4.188$ for $\bar{\Omega} = 0.4$. The damping effect in the deep interior is by a factor of 2 to 3 larger than the excitation near the surface.

It may be instructive to mention a result for low m r modes of more massive stars, since the instability for low frequency oscillation modes weakens as the stellar mass increases. Figure 9 shows $\bar{\omega}_{\rm R}$ of odd r modes with $l' = m = 1$ of $8M_\odot$ main-sequence models from the ZAMS to the TAMS for $\bar{\Omega} = 0.6$, where the small thin and large thick circles indicate pulsationally stable and unstable modes, respectively. For $\bar{\Omega} = 0.6$, high radial order r modes with $l' = m = 2$ and 3 become unstable too in the course of evolution, although only the odd r modes with $l' = m = 1$ become unstable for $\bar{\Omega} = 0.4$.

3.2 Eigenfunctions of buoyant r modes

Let us first show some examples of the eigenfunctions (expansion functions) of low m r modes of the $5M_\odot$ ZAMS star, which consists of the convective core and the radiative envelope that contains two thin convection zones in the outer part of the envelope. Figure 10 depicts the eigenfunction $x\mathrm{Re}(iT_{l'_1})$ of *odd* r modes with $l' = m = 1$ (panel a) and of *even* r modes with $l' = m+1 = 2$ (panel b) for $\bar{\Omega} = 0.4$, where $x = r/R$, and the amplitude normalization is given by $\mathrm{Re}(S_{l_1}) = 1$ at the surface. Note that in the vicinity of the outer boundary of the convective core, the even r modes have a node, which is not necessarily apparent in the figure. Since $\nabla - \nabla_{\rm ad}$ is assumed to vanish in the convective core, $iT_{l'_1}$ is almost constant there (see, e.g., Saio 1982). Although the amplitude of the r_0 mode has the maximum just outside the convective core, the amplitude maximum shifts to the surface, as the radial order n and the number of radial nodes in the radiative envelope increase. It is important to note that for the even r modes with $l' = m+1 = 2$, the isentropic convective core is an evanescent region for the oscillation and no fundamental mode that has no radial nodes of the eigenfunction $\mathrm{Re}(iT_{l'_1})$ exists. We find this is also the case for both even and odd r modes if $l' > |m|$.

Figure 11 shows the eigenfunction $x\mathrm{Re}(iT_{l'_1})$ of odd r modes with $l' = m = 1$ of a $5M_\odot$ model with $\mathrm{Log}T_{\rm eff} = 4.188$ for $\bar{\Omega} = 0.4$, where the long dash-dotted line, short dash-dotted line, dotted line, and solid line indicate r_0, r_1, r_{10} and r_{20} modes, respectively, and the amplitude normalization is given by $\mathrm{Re}(S_{l_1}) = 1$ at the surface. This model has the μ gradient zone just outside the convective core. The fundamental r_0 mode, which is shown in the inlet, behaves like an interface mode and the amplitude has the sharp maximum at the interface between the convective core and the μ-gradient zone. We also note that the high radial order r modes have very short radial wavelengthes in the μ-gradient zone, which leads to the dense frequency spectrum.

4 FORCING ON ROTATION BY BUOYANT R MODES

In the wave-meanflow interaction formalism, every physical quantity of a rotating star is decomposed into the zonally-averaged, axisymmetric part and the non-axisymmetric, residual part, and we regard the former as the quantity in the meanflow and the latter as the one representing waves (oscillations) (e.g., Pedlosky 1987, Andrews, Holton, & Leovy 1987). The forcing equation for stellar rotation may be given by (e.g., Lee & Saio 1993; see also Ando 1983)

$$\frac{\partial}{\partial t}j(r,t) = -\frac{1}{2}\frac{1}{r^2}\frac{\partial}{\partial r}[r^2\left\langle r\sin\theta \mathrm{Re}\left(\bar{\rho}\tilde{v}'_\phi\tilde{v}'^*_r + \bar{v}_\phi\tilde{\rho}'\tilde{v}'^*_r\right)\right\rangle] - \frac{1}{2}\left\langle \mathrm{Re}\left(im\tilde{\rho}'^*\tilde{\Phi}'\right)\right\rangle, \tag{20}$$

where

$$j(r,t) = \langle r\sin\theta\bar{\rho}\bar{v}_\phi\rangle, \quad \bar{v}_\phi = \frac{1}{2\pi}\int_0^{2\pi} v_\phi d\phi, \quad \bar{\rho} = \frac{1}{2\pi}\int_0^{2\pi}\rho d\phi, \tag{21}$$

and

$$\langle\cdots\rangle = \frac{1}{2}\int_0^\pi d\theta\sin\theta(\cdots), \tag{22}$$

and we rewrite the forcing equation (20) as

$$\frac{1}{\tau_0(r)} = \frac{1}{\tau_1(r)} + \frac{1}{\tau_2(r)} + \frac{1}{\tau_3(r)}, \tag{23}$$

where τ's are time scales of local variation of the meanflow defined as

$$\frac{1}{\tau_0(r)} = \frac{1}{j(r,t)}\frac{\partial j(r,t)}{\partial t}, \tag{24}$$

$$\frac{1}{\tau_1(r)} = -\frac{1}{2}\frac{1}{j(r,t)}\frac{1}{r^2}\frac{\partial}{\partial r}[r^2\left\langle r\sin\theta \mathrm{Re}\left(\bar{\rho}\tilde{v}'_\phi\tilde{v}'^*_r\right)\right\rangle], \tag{25}$$

$$\frac{1}{\tau_2(r)} = -\frac{1}{2}\frac{1}{j(r,t)}\frac{1}{r^2}\frac{\partial}{\partial r}[r^2\left\langle r\sin\theta \mathrm{Re}\left(\bar{v}_\phi\tilde{\rho}'\tilde{v}'^*_r\right)\right\rangle], \tag{26}$$

$$\frac{1}{\tau_3(r)} = -\frac{1}{2}\frac{1}{j(r,t)}\left\langle \mathrm{Re}\left(im\tilde{\rho}'^*\tilde{\Phi}'\right)\right\rangle, \tag{27}$$

and positive τ_0 stands for acceleration of the rotation. Note that $\boldsymbol{v}' = \mathrm{i}\omega\boldsymbol{\xi}$ for uniformly rotating stars. The importance of non-conservative (e.g., non-adiabatic) effects accompanied with the oscillation will be apparent by rewriting the Eulerian formulation into a Lagrangian one (e.g, Ando 1986b; see also Andrews & McIntyre 1978). The time derivative of the total angular momentum, $\dot{J}$, may be given by

$$\dot{J} = \int_0^R 4\pi r^2\frac{\partial j}{\partial t}dr = -2\pi R^2\left\langle R\sin\theta \mathrm{Re}\left(\bar{\rho}\tilde{v}'_\phi\tilde{v}'^*_r + \bar{v}_\phi\tilde{\rho}'\tilde{v}'^*_r\right)\right\rangle - \int_0^R 2\pi r^2\left\langle \mathrm{Re}\left(im\tilde{\rho}'^*\tilde{\Phi}'\right)\right\rangle dr, \tag{28}$$

where the first term on the right hand side stands for the angular momentum luminosity, and the second term is the gravitational torque.

In Figure 12, we plot $\tau_j^{-1}(r)$ with j = 0, 1, and 2 versus r/R for a unstable $l' = m = 1$ r_{20} mode of the $5M_\odot$ model with $\mathrm{Log}T_{\mathrm{eff}} = 4.188$ for $\bar{\Omega} = 0.4$, where the solid line, dotted line, and dashed lines represent $\tau_0^{-1}(r)$, $\tau_1^{-1}(r)$, and $\tau_2^{-1}(r)$, respectively, and the amplitude normalization for the mode is given by $\mathrm{Re}(S_{l_1}(R)) = 1$. For self-excited oscillations, the term τ_3^{-1} is negligible compared to the other two terms and is not shown in the figure. Although the term $\tau_2^{-1}(r)$ was ignored in the analysis by Ando (1983), the term for low frequency oscillation modes can be more important than the term τ_1^{-1} in the surface region because of the boundary condition $\delta p = 0$ we apply at the surface. Since $\tau_0^{-1}(r)$ is positive in the region of $r \sim R$, the unstable r_{20} mode contributes to accelerating the surface rotation. This acceleration of the surface rotation is brought about by many unstable $l' = m$ r modes in SPB stars as shown by Figure 13, in which $\tau_0^{-1}(R)$ and $\dot{J}/10^{34}$ for odd r modes with $l' = m = 1$ of the $5M_\odot$ model for $\bar{\Omega} = 0.4$ are plotted versus the dimensionless oscillation frequency $\bar{\omega}_{\mathrm{R}}$. Here, the circles and squares stand for $\tau_0^{-1}(R)$ and $\dot{J}/10^{34}$, respectively, and the filled and open symbols indicate pulsationally unstable and stable modes, respectively. Note that to calculate the quantities $\tau_0^{-1}(R)$ and $\dot{J}$, we have employed the amplitude normalization given by $\mathrm{Re}(S_{l_1}(R)) = 1$ for the modes. We find that $\tau_0^{-1}(R)$ is positive and $\dot{J}$ is negative for the pulsationally unstable $l' = m = 1$ r modes of the model. Negative $\dot{J}$ means a loss of angular momentum from the star, or equivalently a positive angular momentum luminosity through the surface of the star.

The numerical values of $\dot{J}$ in Figure 13 can be compared with observationally estimated ones. The amount of angular momentum supply in a unit time necessary to sustain a decretion disc around the central star in a Be system may be estimated as (e.g., Lee, Saio, & Osaki 1991)

$$\dot{J}_D = \dot{M}_D\sqrt{GMR} = 1.9\times10^{34}\frac{\dot{M}_D}{10^{-10}M_\odot/yr}\left(\frac{M}{M_\odot}\right)^{1/2}\left(\frac{R}{R_\odot}\right)^{1/2}, \tag{29}$$

where $\dot{M}_D$ denotes the mass decretion rate through the disc, and M and R are the mass and radius of the central star, and an estimation of $\dot{M}_D \sim 10^{-10} M_\odot/yr$ given by Okazaki (2001) has been used. Since the quantity $\dot{J}$ defined in equation (28) is proportional to the sqaure of the oscillation amplitudes, if we consider the typical value of $\dot{J}_D$ is of order of 10^{35} to 10^{36} for a decretion disc in Be stars, the oscillation amplitudes of order of $\mathrm{Re}(S_{l_1}(R)) = 0.01 \sim 0.1$ may be able to produce $\dot{J}$ comparable to the observational estimations $\dot{J}_D$.

5 COMPARISON WITH THE TRADITIONAL APPROXIMATION

It may be appropriate here to make a brief comparison between numerical results obtained with and without the traditional approximation for r mode oscillations of rotating stars. In this section, for both calculations with and without the traditional approximation, we consistently employ the Cowling approximation, neglecting the Eulerian perturbation of the gravitational potential.

The traditional approximation has been used by several authors (e.g., Ushomirsky & Bildsten 1998, Townsend 2005a,b; Savonije 2005) to numerically investigate low frequency oscillations of SPB stars. Under the traditional approximation, we ignore the local horizontal component of the rotation vector $\mathbf{\Omega}$ in the momentum conservation equation. Adiabatic oscillation equations in the Cowling approximation then becomes self-ajoint, and separation of variables becomes possible between spherical polar coordinates (r, θ, ϕ) so that an oscillation mode of a rotating star can be represented by

$$p'(r,\theta,\phi,t) = p'_{kmn}(r) H_{km}(\cos\theta) e^{\mathrm{i}m\phi + \mathrm{i}\sigma t}, \tag{30}$$

where n denotes the radial order, and the Hough function $H_{km}(\cos\theta)$ with integer indices k and m is the solution to Laplace's tidal equation and depends on the ratio $2\Omega/\omega$ (e.g., Bildsten, Ushomirsky, & Cutler 1996; Lee & Saio 1997). This separation of variables greatly simplifies the problem of analyzing numerically and analytically low frequency oscillations of rotating stars, although couplings between oscillation modes associated with different Hough functions cannot be treated under the approximation. In geophysics, the traditional approximation has long been used to discuss low frequency atmospheric or ocean waves that satisfy $N/\omega >> 1$ and have the horizontal velocity much larger than the vertical (radial) velocity (e.g., Eckart 1960). Although atmospheric or ocean waves discussed in geophysics are propagating in a layer much thinner compared to the radius of the earth, low frequency modes of a rotating star in general have eigenfunctions extending from the center to the surface of the star and do not always satisfy in the interior the conditions needed for the tradiational approximation to be valid.

A typical difficulty in applying the traditional approximation to stellar pulsations appears in spurious singular behavior of the eigenfunctions at the center for certain groups of low frequency modes. In the tradiational approximation, the governing equations for adiabatic oscillations may be given by (e.g., Lee & Saio 1987a)

$$r\frac{dz_1}{dr} = \left(\frac{V}{\Gamma_1} - 3\right) z_1 + \left(\frac{\lambda_{km}}{c_1\bar{\omega}^2} - \frac{V}{\Gamma_1}\right) z_2, \tag{31}$$

$$r\frac{dz_2}{dr} = \left(c_1\bar{\omega}^2 - rA\right) z_1 + (1 - rA - U)\, z_2, \tag{32}$$

where the variables z_1 and z_2 respectively correspond to ξ_r/r and $p'/\rho g r$, and λ_{km} is the separation factor, which depends on the ratio $\nu \equiv 2\Omega/\omega$ for given integer indices m and k, and

$$U = \frac{d\ln M_r}{d\ln r}, \quad V = -\frac{d\ln p}{d\ln r}, \quad rA = \frac{d\ln\rho}{d\ln r} - \frac{1}{\Gamma_1}\frac{d\ln p}{d\ln r}, \quad c_1 = \frac{(r/R)^3}{M_r/M}, \tag{33}$$

and $M_r = \int_0^r 4\pi r^2 \rho dr$. Here, we have used the notation for λ_{km} employed by Lee & Saio (1997). For $k \geq 0$, $\lambda_{km} \geq 0$ tends to $(|m|+k)(|m|+k+1)$ as $\nu \to 0$, while for $k < 0$, we have branches of ν, in which λ_{km} is negative. R modes are associated with λ_{km} with negative k that is positive for $\omega < 2m\Omega/[l'(l'+1)]$ where $l' = m + |k+1|$. Assuming both z_1 and z_2 in equations (31) and (32) are proportional to r^β in the vicinity of the stellar centre, we obtain the regularity condition at the centre for the functions z_1 and z_2 given by

$$\beta = (-5 + \sqrt{1 + 4\lambda_{km}})/2 \equiv \tilde{l} - 2 \geq -1, \tag{34}$$

which is rewritten as

$$\lambda_{km} = \tilde{l}(\tilde{l}+1) \geq 2. \tag{35}$$

As suggested by Figure 1 of Lee & Saio (1997), prograde modes associated with $k = 0$ and $m = 1$ and r modes with $k \leq -1$ except for high radial order $k = -1$ r modes do not satisfy the condition (35), and they show spurious singular behavior of the eigenfunctions z_1 and z_2 at the center that does not exist without the traditional approximation.

To avoide this mode-dependent, awkward singular behavior we meet when numerically integrating the oscillation equations (31) and (32), Townsend (2005a,b) introduced a new set of dependent variables q_1 and q_2 defined by

$$z_1 = q_1 x^\beta, \quad z_2 = q_2 x^\beta, \tag{36}$$

to obtain

$$r\frac{dq_1}{dr} = \left(\frac{V}{\Gamma_1} - 3 - \beta\right) q_1 + \left(\frac{\lambda_{km}}{c_1\bar{\omega}^2} - \frac{V}{\Gamma_1}\right) q_2, \tag{37}$$

$$r\frac{dq_2}{dr} = \left(c_1\bar{\omega}^2 - rA\right) q_1 + (1 - rA - U - \beta)\, q_2, \tag{38}$$

where $x = r/R$. Obviously, the variables q_1 and q_2 are always regular at the stellar center, and we have no trouble to solve numerically equations (37) and (38) to obtain eigenfrequencies ω of low frequency modes.

Under the traditioanl approximation, Townsend (2005a,b) numerically solved a set of coupled linear ordinary differential equations derived by using regularized dependent variables like q_1 and q_2 for adiabatic and non-adiabatic oscillations. Here, we calculate non-adiabatic r modes of the $5M_\odot$ ZAMS model with $Z = 0.02$, following the formulation given by Townsend (2005a), and we compare the results to those computed without the traditional approximation. Figure 14 shows $\bar{\omega}_{\rm R}$ (panel a) and the growth rate $|\eta|$ (panel b) of odd r modes with $l' = m = 1$ versus the radial order n for $\bar{\Omega} = 0.4$. From panel (a), we find that the two calculations for $\bar{\omega}_{\rm R}$ are qualitatively in good agreement with each other, but it is also apparent that the difference in $\bar{\omega}_{\rm R}$ between the two calculations for a given radial order n becomes comparable to the difference in $\bar{\omega}_{\rm R}$ between two consecutive radial order modes as the radial order n increases. Panel (b), on the other hand, shows that the growth rates of unstable r modes obtained in the traditional approximation are systematically smaller and the instability band in the radial order n is narrower, compared to those obtained without the approximation. We also find that the fundamental r_0 mode is unstable in the traditional approximation, but it is not without the approximation. This difference in the stability of the fundamental r modes may be attributable to the singular behavior of the eigenfunctions in the traditional approximation, since the large amplitudes of the eigenfunctions may wrongly strengthen the instability in the convective core.

Figure 15 plots $\bar{\omega}_{\rm R}$ versus the radial order n for *even* r modes with $l' = m + 1 = 2$ for $\bar{\Omega} = 0.4$, where the small filled and large open circles stand for the results with and without the traditional approximation, respectively. Although the two calculations of $\bar{\omega}_{\rm R}$ are in reasonable agreement, it is interesting to note that in the traditional approximation there exists the fundamental r_0 mode with even parity, which does not exist if we lift the traditional approximation.

In Figure 16, we plot ${\rm Re}(\lambda_{km})$ versus the radial order n of r modes, where the filled and open circles respectively stand for *odd* r modes with $l' = m = 1$ and *even* r modes with $l' = m + 1 = 2$ for $\bar{\Omega} = 0.4$. Note that the former and the latter corresponds to $(k, m) = (-1, 1)$ and $(-2, 1)$, respectively, since $l' = |m| + |k + 1|$ for r modes. The figure clearly shows that the low radial order r modes with $l' = m = 1$ and all the r modes with $l' = m + 1 = 2$ do not satisfy the regularity condition ${\rm Re}(\lambda_{km}) \geq 2$ for the functions z_1 and z_2 at the center. As an example, Figure 17a depicts the eigenfunctions $x{\rm Re}(z_1)$ and $x{\rm Re}(S_{l_1})$ for the fundamental r modes with $l' = m = 1$, while Figure 17b shows the eigenfunctions for r_{10} modes with $l' = m = 1$, where $\bar{\Omega} = 0.4$, and the functions z_1 and S_{l_1} are obtained with and without the traditional approximation, and the amplitude normalization for z_1 and S_{l_1} is given by ${\rm Re}(z_1) = 1$ and ${\rm Re}(S_{l_1}) = 1$ at the surface. The function xz_1 of the fundamental mode is singular at the stellar center, but xS_{l_1} is not. On the other hand, no singular behavior appears for the high radial order r_{10} modes with $l' = m = 1$ even in the traditional approximation.

It seems pulsational instability of r modes appears weaker in the traditional approximation. This trend can be seen more clearly in pulsational stability of low m r modes of more massive stars as shown by Figure 18, in which $\bar{\omega}_{\rm R}$ of $l' = m = 1$ r modes computed for $8M_\odot$ main-sequence models in the traditional approximtioan is plotted versus ${\rm Log}T_{\rm eff}$ for $\bar{\Omega} = 0.6$, where the samll open circles and large filled circles stand for stable and unstable modes, respectively. Camparing Figure 18 with Figure 9, we find the instability domain in the traditional approximation is largely shrinked and the blue edge of the instability strip has shifted to the lower $T_{\rm eff}$ in the HR diagram.

6 CONCLUSIONS

In this paper, we have calculated nonadiabatic r modes of SPB stars with mass ranging from $M = 3M_\odot$ to $M = 8M_\odot$, and found that low m, odd r modes with $l' = m$ become pulsationally unstable if we assume rapid rotation of the stars, confirming the numerical results obtained in the traditional approximation by Savonije (2005) and Townsend (2005b). No low m, even r modes with $l' = m + 1$ are found pulsationally unstable, which contradicts Savonije (2005) who found unstable even r modes. A possible reason for the contradiction may be that Sovonije (2005) calculated forced oscillations for r modes of SPB stars, which are not necessarily equivalent to free r mode oscillations computed in this paper. Photometric amplitudes of the variability caused by unstable odd r modes with $l' = m$ will be strongly dependent on the inclination angle between the rotation axis and the line of sight, because the surface pattern of the temperature perturbation is antisymmetric about the equator of the star. Applying the wave-meanflow formalism to pulsationally unstable r modes in SPB stars, we have found that the unstable r modes have a contribution to accelerating the surface rotation of the star. Note that it is also important to examine the mechanism for unstable g modes.

We have made a brief comparison between r mode calculations done with and without the traditional approximation. We found that the oscillation frequency $\omega_{\rm R}$ of r modes obtained in the traditional approximation are qualitatively in good agreement with those without the traditional approximation. The growth rates of unstable r modes in the traditional approximation are systematically smaller than those obtained without the traditional approximation, that is, the pulsational instability appears weaker in the traditional approximation. For r modes associated with $\lambda_{km} < 2$, the eigenfunctions obtained in the traditional approximation show spurious singularity at the center, which may affect the pulsational stability, particularly for the low radial order modes. Note that we need to make a comparison for the case of g modes to have a good understanding about the validity of the traditional approximation. For low frequency g modes, mode coupling between g modes associated with different λ_{km}'s might have significant influence on the frequency spectrum and the stability, as suggested by Lee (2001). For inertial modes in an isentropic star for whcih the Brunt-Väisälä frequency N vanishes identically in the interior, we found it difficult to obtain the oscillation frequencies in general. This is quite reasonable because the traditional approximation is considered to be valid for low frequency modes with $N/\omega >> 1$. Interestingly enolugh, however, we do obtain the frequencies corresponding to the fundamental r modes with $l' = m$ for isentropic polytropes even in the traditional approximation. The frequency ω of the r mode in the traditional approximtion is very close to $2\Omega/(|m| + 1)$, which is consistent with previous calcualtions done without the traditional approximation (e.g., Yoshida & Lee 2000a).

Theoretically speaking, both g modes and r modes are excited in rapidly rotating SPB stars. As shown by Aerts et al (1999), a fraction of SPB stars are rapid rotators, and we think it is tempting to look for a link between Be stars and raidly rotating SPB stars. Recent discovery of a Be star that also shows SPB variability caused by g modes and r modes (private communication with G. Walker and with H. Saio, 2005) indicates such a possibility. If low m r modes excited in SPB stars accelerate the surface rotation effectively as a result of angular momentum redistribution in the interior, this acceleration can be a candidate mechanism for disc formation around the rapidly rotating star. We speculate unstable r modes are a steady supplier of angular momentum to the disc and prograde and retrograde g modes also excited in SPB stars may cause quasi-periodic pheonomena in Be stars. Further theoretical and observational studies are warranted.

REFERENCES

Aerts C., De Cat P., Peeters E., Decin L., De Ridder J., Kolender K., Meeus K., Van Winckel H., Cuypers J., Waelkens C., 1999, A&A, 343, 872
Ando H., 1981, MNRAS, 197, 1139
Ando H., 1982, A&A, 108, 7
Ando H., 1983, PASJ, 35, 343
Ando H., 1986, A&A, 163, 97
Ando H., 1986, in Hydrodynamic and Magnetodynamic Problems in the Sun and Stars, ed. by Osaki, Y., University of Tokyo Press, Tokyo
Andrews D.G., McIntyre M.E., 1978, J. Atmos. Sci., 35, 175
Andrews D.G., Holton J.R., Leovy C.B., 1987, Middle Atmosphere Dynamics, Academic Press
Berthomieu G., Gonczi G., Graff Ph., Provost J., Rocca A., 1978, A&A, 70, 597
Berthomieu G., Provost J., 1983, A&A, 122, 199
Bildsten L., Ushomirsky G., Cutler C., 1996, ApJ, 460, 827
Craik A.D.D., 1985, Wave Interactions and Fluid Flows, Cambridge University Press, Cambridge
Dziembowski W.A., Pamyatnykh A.A., 1993, MNRAS, 262, 204
Dziembowski W.A., Moskalik P., Pamyatnykh A.A., 1993, MNRAS, 265, 588
Eckart C., 1960, Hydrodynamics of Ocean and Atmospheres, Pergamon Press, Oxford
Gautschy A., Saio H., 1993, MNRAS, 267, 1071
Iglesias C.A., Rogers F.J., 1996, ApJ, 464, 943
Iglesias C.A., Rogers F.J., Wilson B.G., 1992, ApJ, 397, 717
Kiriakidis M., El Eid M.F., Glatzel W., 1992, MNRAS, 255, 1
Lee U., 2001, ApJ, 557, 311
Lee U., Saio H., 1987a, MNRAS, 224, 513
Lee U., Saio H., 1987b, MNRAS, 225, 643
Lee U., Saio H., 1997, ApJ, 491, 839
Lee U., Saio H., 1993, MNRAS, 261, 415
Lee U., Saio H., Osaki Y., 1991, MNRAS, 250, 432
Lighthill J., 1978, Waves in Fluids, Cambridge Univ. Press, Cambridge
Lindzen R.S., Holton J.R., 1968, J. Atmos. Sci., 25, 1095
Lockitch K.H., Friedman J.L., 1999, ApJ, 521, 764
Okazaki A.T., 2001, PASJ, 53, 119
Osaki Y., 1986, PASP, 98, 30
Papaloizou J., Pringle J.E., 1978, MNRAS, 182, 423
Pedlosky J., 1987, Geophysical Fluid Dynamics, 2nd edn, Springer-Verlag, Hidelberg
Plumb R.A., 1977, J. Atomos. Sci., 34, 1847
Porter J.M., RiviniusT., 2003, PASP, 115, 1153
Provost J., Berthomieu G., Rocca A., 1981, A&A, 94, 126
Saio H., 1982, ApJ, 256, 717
Savonije G.J., 2005, astro-ph/0506153
Townsend R.H.D., 2005, MNRAS, 360, 465
Townsend R.H.D., 2005, astro-ph/0506580
Unno W., Osak Y., Ando H., Saio H., Shibahashi H., 1989, Nonradial Oscillations of Stars, 2nd edn. University of Tokyo Press, Tokyo
Ushomirsky G., Bildsten L., 1998, ApJ, 497, L101
Waelkens C., 1991, A&A, 246, 453
Waelkens C., Aerts C., Kestens E., Crenon M., Eyer L., 1998, A&A, 330, 215
Yoshida S., Lee U., 2000a, ApJ, 529, 997
Yoshida S., Lee U., 2000b, ApJS, 129, 353

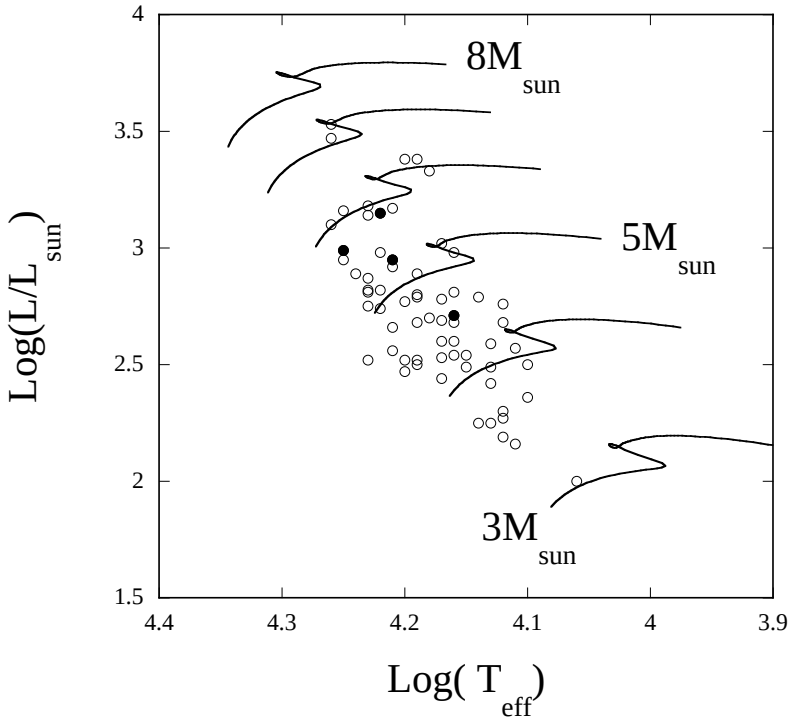

Figure 1. Evolution tracks of main-sequence stars with mass ranging from $3M_\odot$ to $8M_\odot$ for $X = 0.7$ and $Z = 0.02$. The circles stand for SPB stars tabulated in Waelkens et al (1998), and the filled circles indicate rapidly rotating SPB stars as classified by Aerts et al (1999).

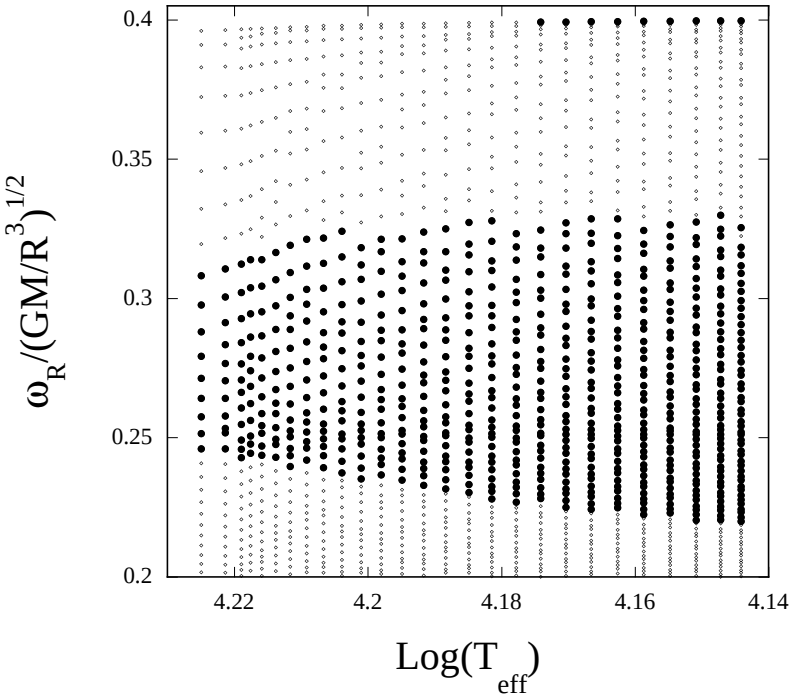

Figure 2. $\bar{\omega}_{\rm R} = \omega_{\rm R}/\sqrt{GM/R^3}$ versus Log$T_{\rm eff}$ for odd r modes with $l' = m = 1$ of $5M_\odot$ main-sequence models for $\bar{\Omega} = \Omega/\sqrt{RM/R^3} = 0.4$. The small thin circles and large thick circles stand for pulsationally stable and unstable modes, respectively.

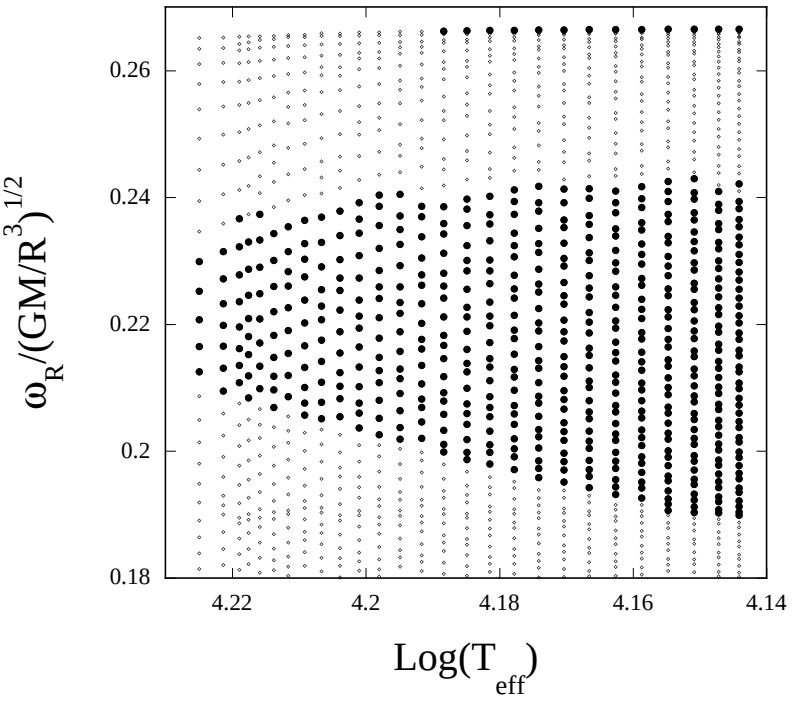

Figure 3. Same as Figure 2 but for odd r modes with $l' = m = 2$.

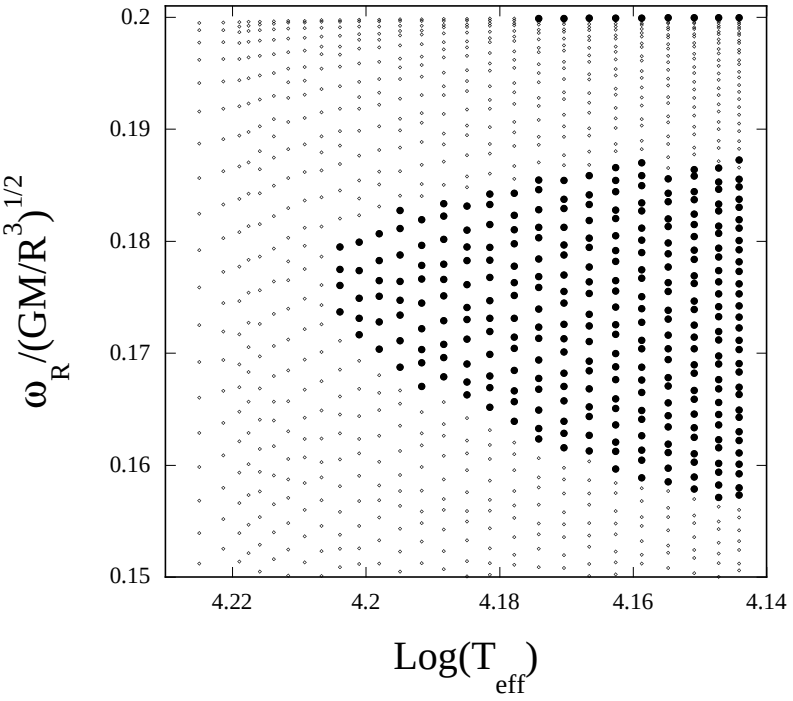

Figure 4. Same as Figure 2 but for $\bar{\Omega} = 0.2$.

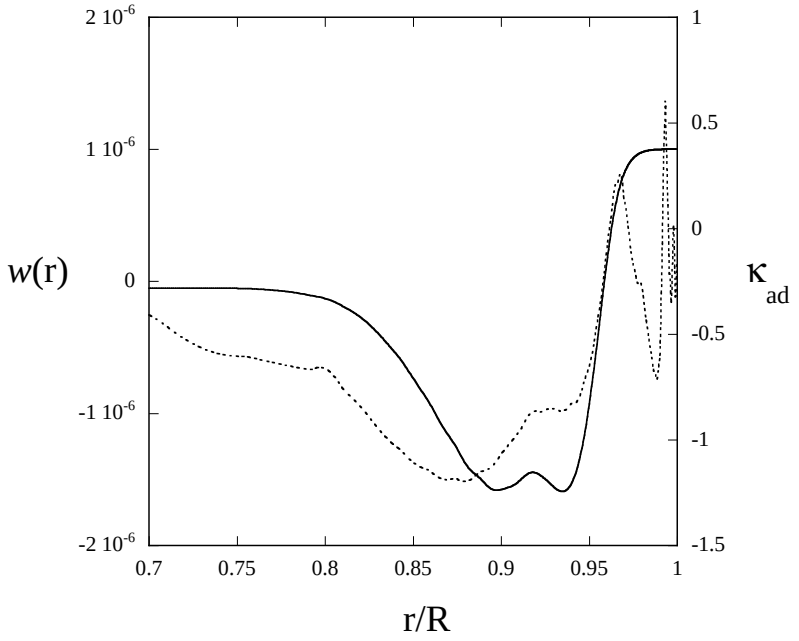

Figure 5. Work integral $w(r)$ of a $l' = m = 1$ r_{20} mode and $\kappa_{\rm ad} = (\partial \ln \kappa / \partial \ln p)_s$ for a $5M_\odot$ model with $\mathrm{Log}(T_{\rm eff}) = 4.188$, where $\bar{\Omega} = 0.4$ is assumed for the mode. Here, the solid and dotted lines are for $w(r)$ and $\kappa_{\rm ad}$, respectively.

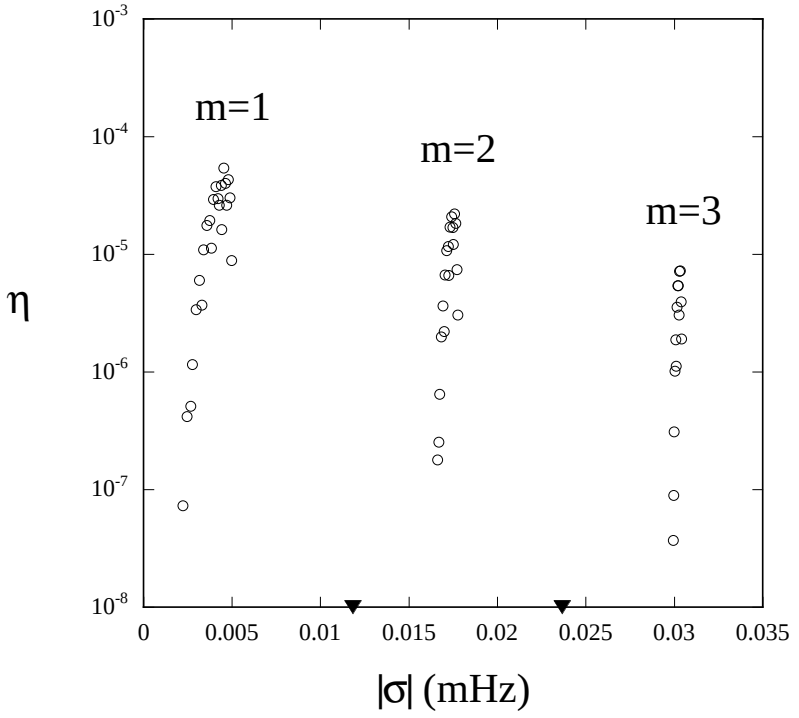

Figure 6. Growth rate $\eta = -\omega_{\rm I}/\omega_{\rm R}$ versus the inertial frame oscillation frequency $|\sigma|$ of unstable odd r modes with $l' = m = 1$, 2, and 3 for a $5M_\odot$ model with $\mathrm{Log}(T_{\rm eff}) = 4.188$, where $\bar{\Omega} = 0.4$ (0.0118mHz). The two filled wedges on the horizontal axis stand for Ω and 2Ω.

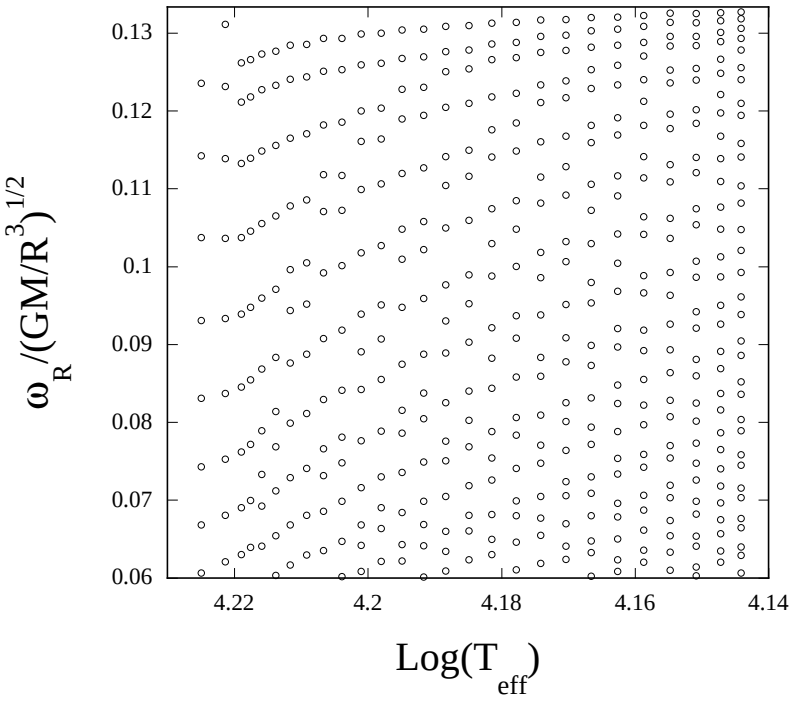

Figure 7. Same as Figure 2 but for even r modes with $l' = m + 1 = 2$. No even r modes with $l' = m + 1 = 2$ are found pulsationally unstable.

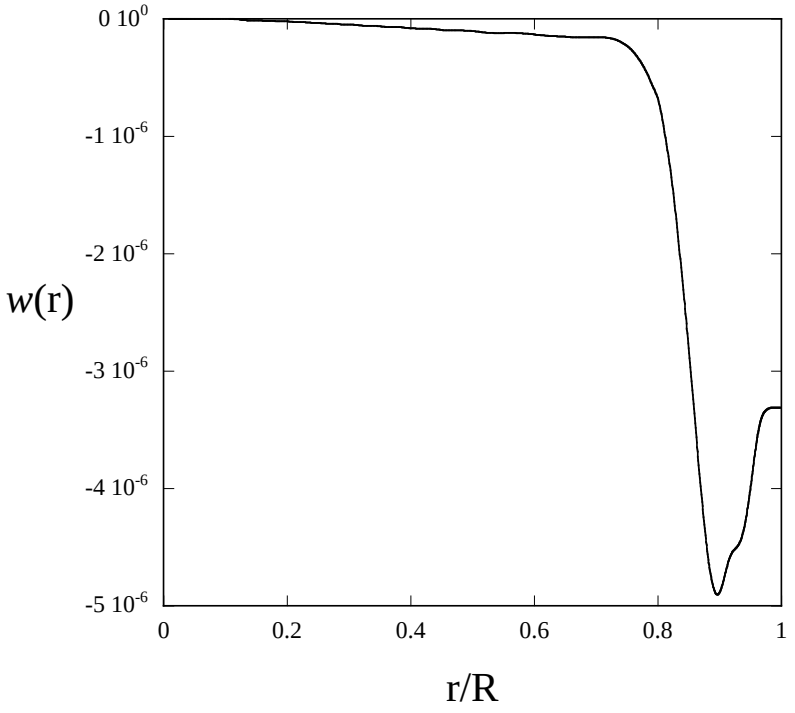

Figure 8. Work integral $w(r)$ of an even $l' = m+1 = 2$ r_{20} mode of a $5M_\odot$ main-sequence model with $\mathrm{Log}(T_{\rm eff}) = 4.188$, where $\bar{\Omega} = 0.4$.

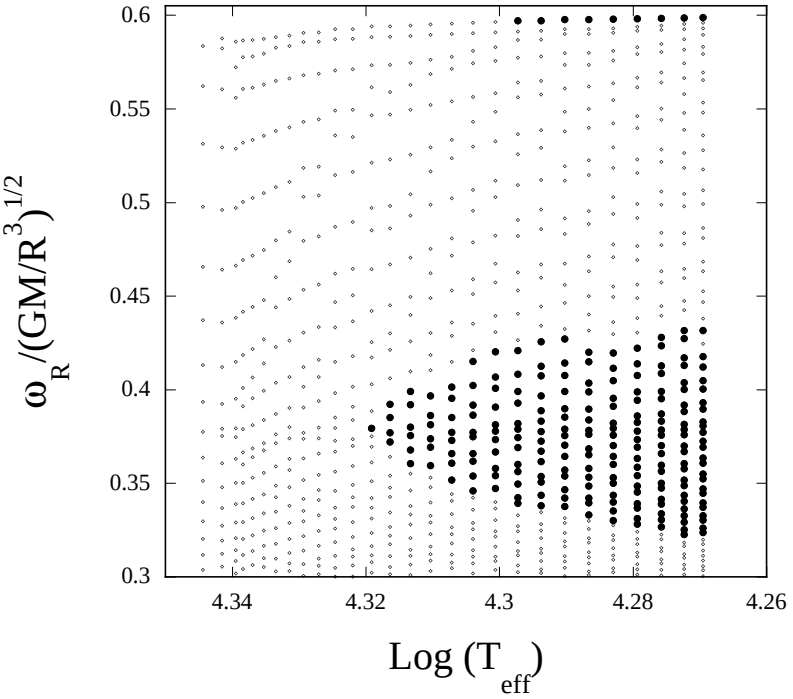

Figure 9. $\bar{\omega}_{\rm R}$ versus Log$T_{\rm eff}$ for odd r modes with $l' = m = 1$ of $8M_\odot$ main-sequence models for $\bar{\Omega} = 0.6$. The small thin circles and large thick circles stand for pulsationally stable and unstable modes, respectively.

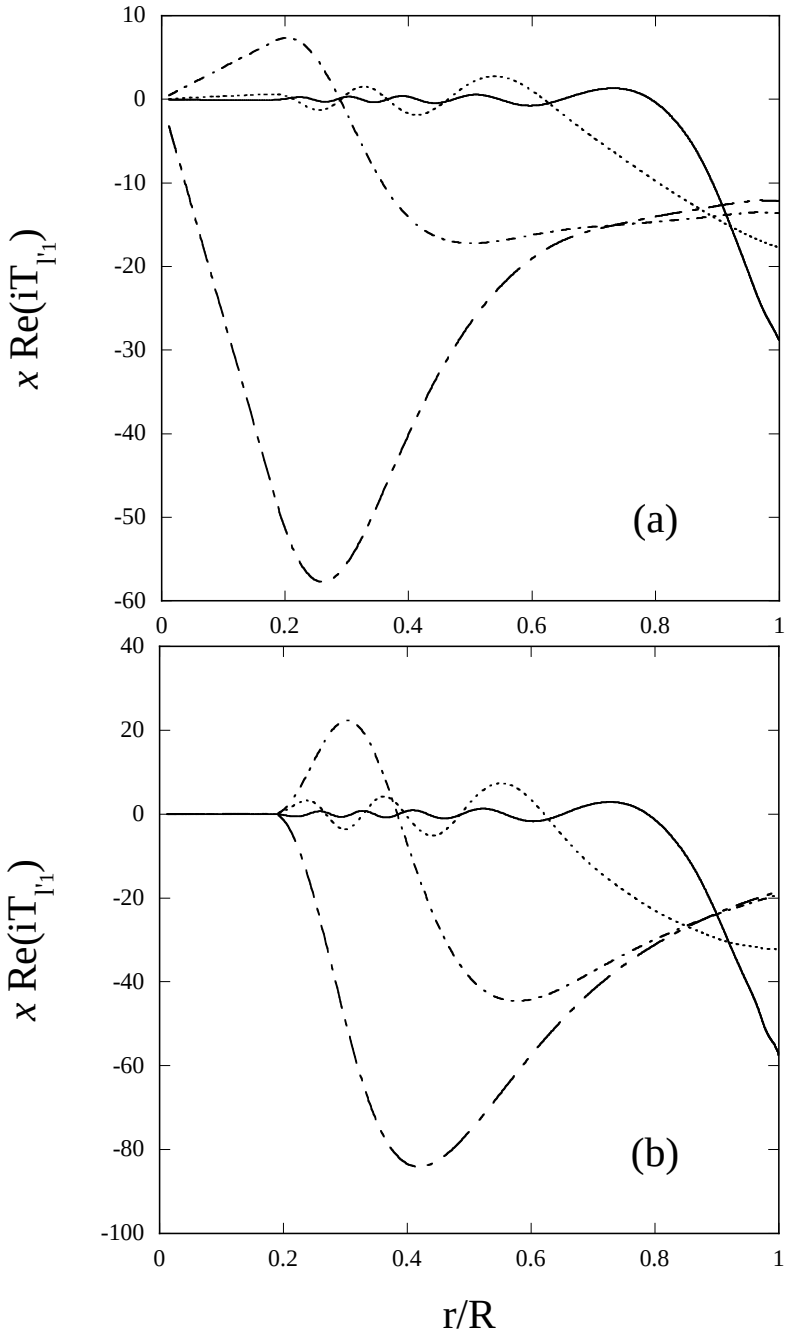

Figure 10. Eigenfunctions $x\mathrm{Re}(\mathrm{i}T_{l'_1})$ versus the fractional radius $x = r/R$ for odd $l' = m = 1$ r modes (panel a) and for even $l' = m + 1 = 2$ r modes (panel b) of the $5M_\odot$ ZAMS model, where $\bar{\Omega} = 0.4$. In panel (a), the long dash-dotted line, short dash-dotted line, dotted line, and solid line represent r_0, r_1, r_5, and r_{10} modes, respectively. In panel (b), the long dash-dotted line, short dash-dotted line, dotted line, and solid line stand for r_1, r_2, r_6,and r_{11} modes, respectively. The amplitude normalization is given by $\mathrm{Re}(S_{l_1}) = 1$ at the surface of the star.

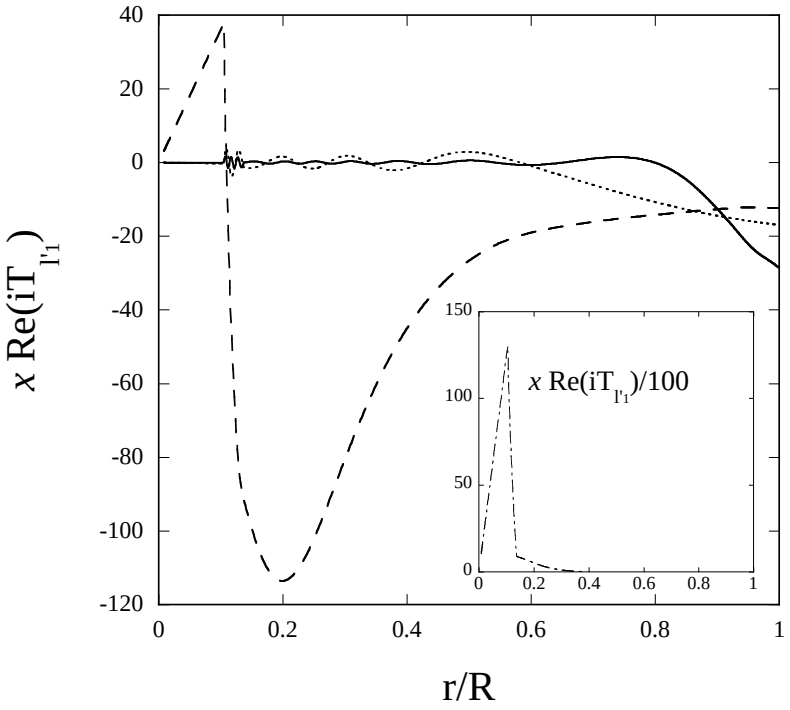

Figure 11. Eigenfunctions $x\mathrm{Re}(\mathrm{i}T_{l'_1})$ versus $x = r/R$ for odd $l' = m = 1$ r modes of a $5M_\odot$ model with $\mathrm{Log}(T_{\rm eff}) = 4.188$, where $\bar{\Omega} = 0.4$. Here, the dash-dotted line, dashed line, dotted line, and solid line represent r_0, r_1, r_{10}, and r_{20} modes, respectively. The inlet shows r_0 mode. The amplitude normalization is given by $\mathrm{Re}(S_{l_1}) = 1$ at the surface of the star.

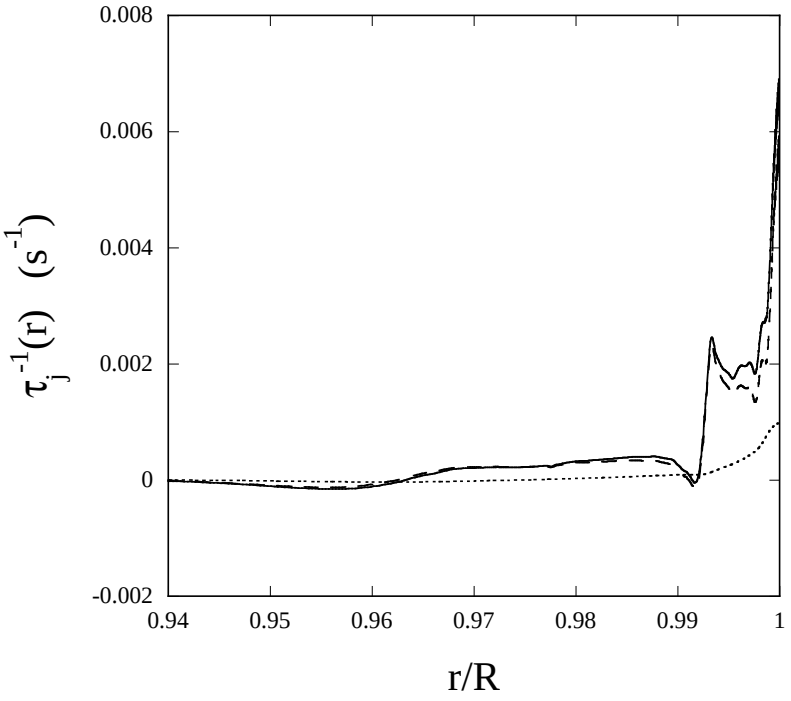

Figure 12. $\tau_j^{-1}(r)$ versus r/R for an odd $l' = m = 1$ r_{20} mode of a $5M_\odot$ main-sequence model with $\mathrm{Log}(T_{\rm eff}) = 4.188$ for $\bar{\Omega} = 0.4$, where the solid line, dotted line, and dashed line stand for τ_0^{-1}, τ_1^{-1}, and τ_2^{-1}, respectively. The amplitude normalization to calculate the r_{20} mode is given by $\mathrm{Re}(S_{l_1}) = 1$ at the surface of the star.

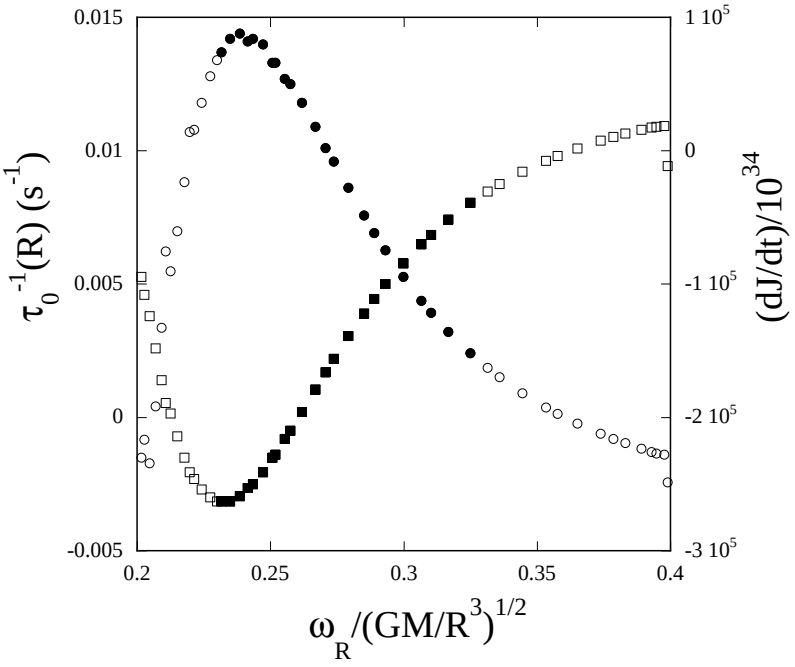

Figure 13. $\tau_0^{-1}(R)$ and $\dot{J}$ versus $\bar{\omega}_{\rm R}$ for odd r modes with $l' = m = 1$ of a $5M_\odot$ main-sequence model with $\mathrm{Log}(T_{\rm eff}) = 4.188$ for $\bar{\Omega} = 0.4$, where the circles and squares stand for $\tau_0^{-1}(R)$ and $\dot{J}$, respectively, and the open and solid symbols indicate pulsationally stable and unstable modes, respectively. The amplitude normalization to calculate the r modes is given by $\mathrm{Re}(S_{l_1}) = 1$ at the surface of the star.

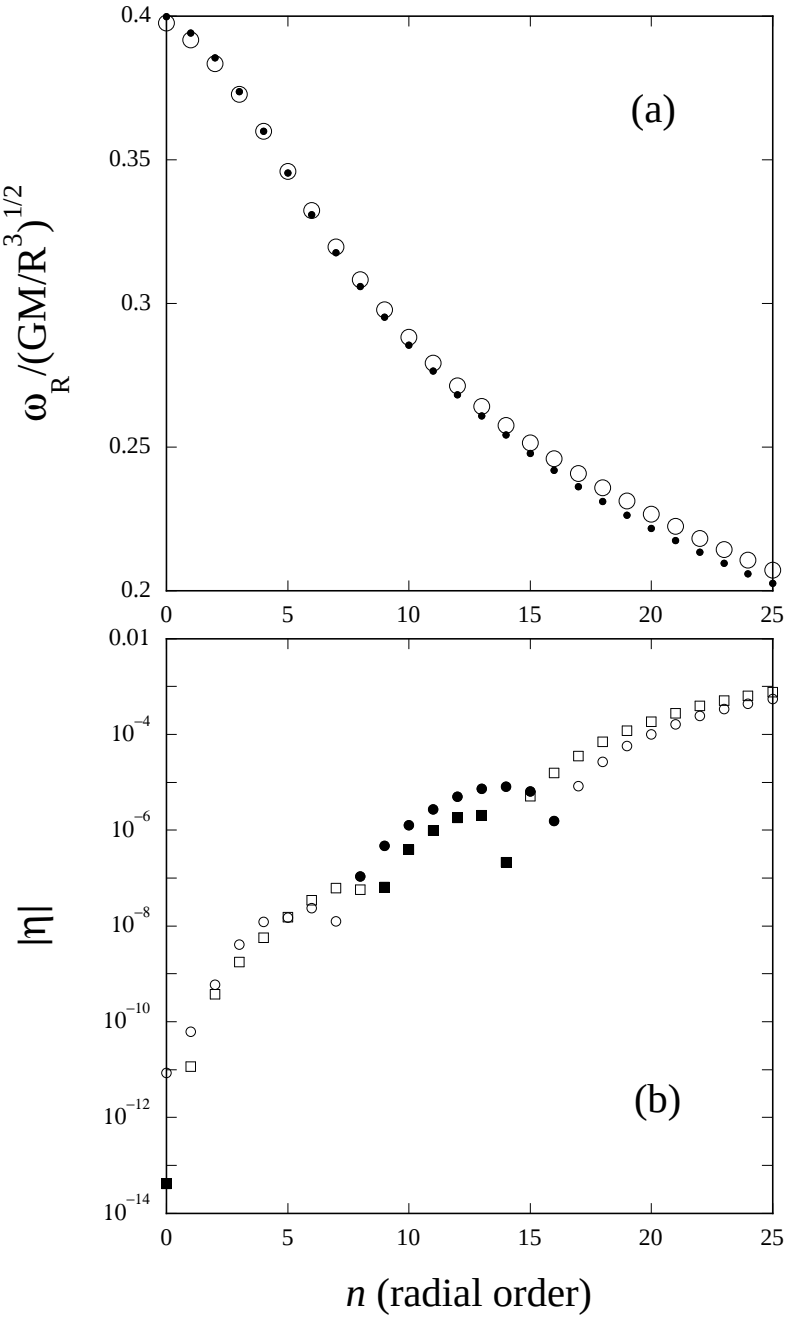

Figure 14. $\bar{\omega}_{\rm R}$ and growth rate $|\eta|$ versus the radial order n of $l' = m = 1$ r modes of the $5M_\odot$ ZAMS model for $\bar{\Omega} = 0.4$. In panel (a), the small filled circles and large open circles stand for results obtained with and without the traditional approximation, respectively. In panel (b), the squares and circles stand for results obtained with and without the traditional approximation, respectively, and the filled and open symbols indicate pulsationally unstable and stable modes, respectively.

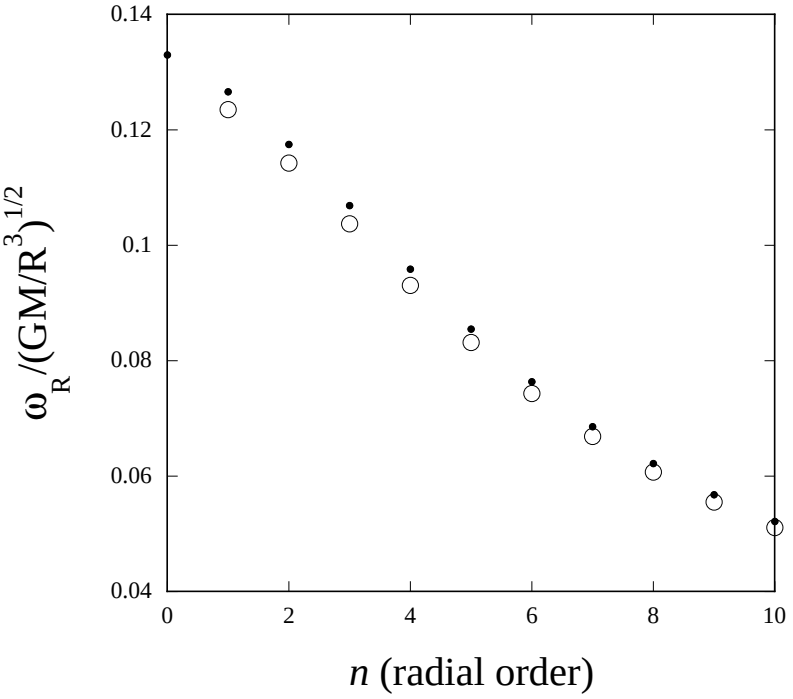

Figure 15. Same as Figure 14a but for even r modes with $l' = m + 1 = 2$.

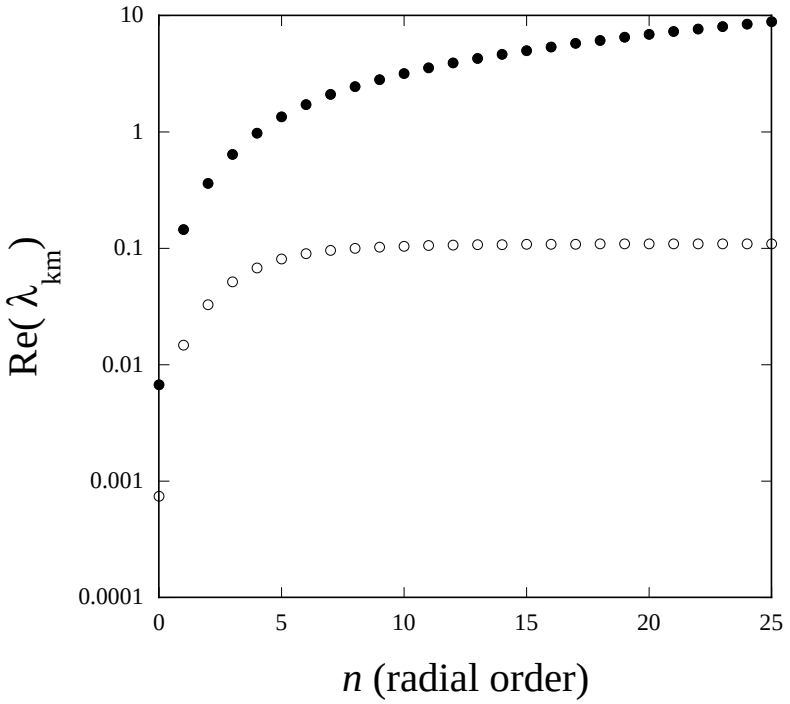

Figure 16. Separation factor λ_{km} versus the radial order n of r modes with $(k, m) = (-1, 1)$ (filled circles) and $(-2, 1)$ (open circles), computed in the traditional approximation for the $5M_\odot$ ZAMS model for $\bar{\Omega} = 0.4$. The r modes associated with $(k, m) = (-1, 1)$ and $(-2, 1)$ correspond to those with $l' = m = 1$ and $l' = m + 1 = 2$, respectively.

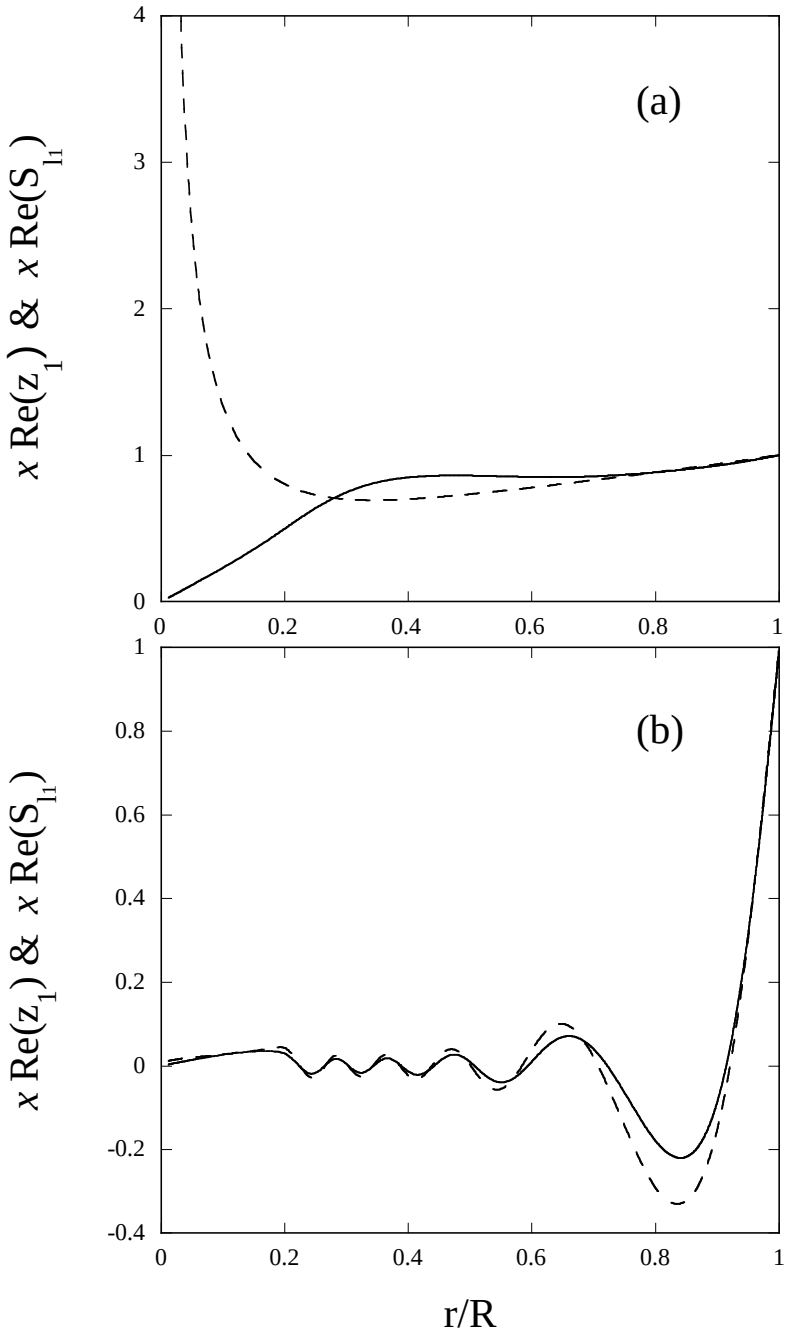

Figure 17. Eigenfunctions $x\mathrm{Re}(S_{l_1})$ (solid line) and $x\mathrm{Re}(z_1)$ (dashed line) are given versus $x = r/R$ for the fundamental r_0 modes with $l' = m = 1$ (panel a) and for r_{10} mode with $l' = m = 1$ (panel b) of the $5M_\odot$ ZAMS model, where $\bar{\Omega} = 0.4$. The eigenfunctions S_{l_1} and z_1 are computed without and with the traditional approximation, respectively. The amplitude normalization is given by $\mathrm{Re}(S_{l_1}) = 1$ and by $\mathrm{Re}(z_1) = 1$ at the surface of the star.

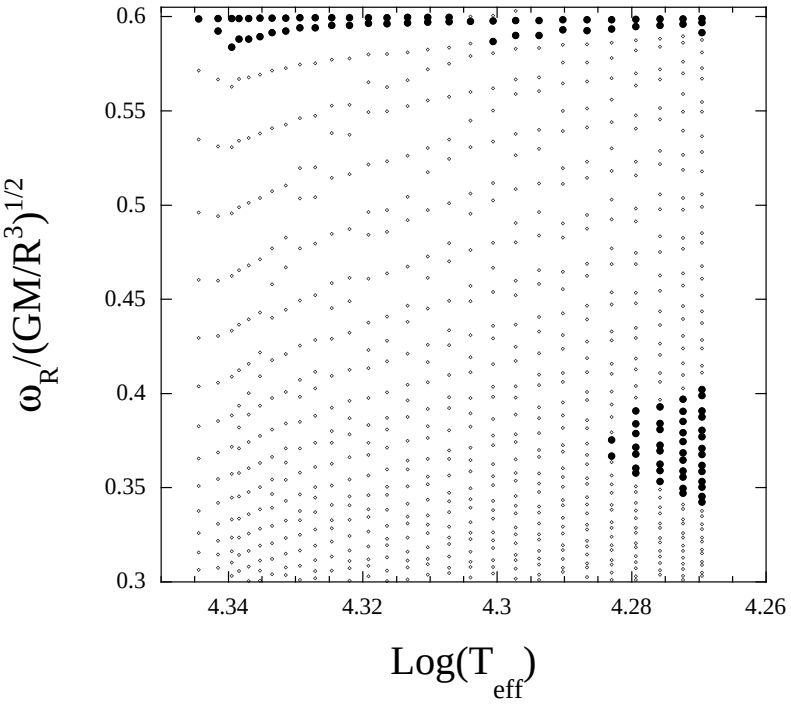

Figure 18. Same as Figure 9 but for r modes computed in the traditional approximation.